Food Structure 32 (2022) 100257

Contents lists available at ScienceDirect

Food Structure

journal homepage: www.elsevier.com/locate/foostr

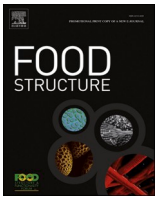

Elastic reinforcement and yielding of starch-filled lipid gels

Braulio A. Macias-Rodriguez [a,b,*], Krassimir P. Velikov [a,b,c]

[a] Unilever Innovation Centre Wageningen, Bronland 14, 6708 WH Wageningen, The Netherlands
[b] Institute of Physics, University of Amsterdam, Science Park 904, 1098 XH Amsterdam, The Netherlands
[c] Soft Condensed Matter, Debye Institute for Nanomaterials Science, Utrecht University, Princetonplein 5, 3584 CC Utrecht, The Netherlands

ARTICLE INFO

Keywords:
Starch
Lipid
Granular
Colloidal
Gel
Random-closed-packing

ABSTRACT

Many foods involve complex suspensions of assorted particles in a Newtonian liquid or viscoelastic medium. In this work, we study the case of suspensions of non-Brownian non-interacting rigid particles: starch, embedded in a soft solid: a colloidal lipid gel. We relate the macroscopic properties of the suspensions to the mechanics of the colloidal gel and the particle volume fraction. As particle volume fraction increases, the suspension gradually stiffens and becomes brittle as the system approaches its maximum packing fraction. The latter is independently determined from a geometric theory of random close packing for polydisperse hard spheres based on the log normal distribution of starch particles dispersed in oil. The elastic modulus, yield stress and yield strain are interrelated through simple scaling laws from a micromechanical homogenization analysis of hard spheres isotropically-distributed in yield stress fluids.

1. Introduction

Structured foods often comprise particulate fillers dispersed in a continuous matrix. For example, confectionery and savory foods, and plant-based meats include suspensions of hydrophilic particles: sugar, salt or texturized protein grains, and hydrophobic particles: cocoa crumbs, dispersed in hydrophobic lipid phases or hydrophilic protein, biopolymer phases or mixtures thereof. The nature of the filler, e.g. shape, rigidity and surface texture, and particle physical interactions, e.g. filler-filler or filler-matrix interactions, have profound effects on mechanical properties (Wijmans and Dickinson 1998; Heinrich et al., 2002; Genovese, 2012). Added to these effects, the physical properties of continuous or filler phases, e.g. phase volume, and phase transitions, e.g. gelation, can change during processing or consumption due to solvent uptake and thermal gradients.

A first step towards understanding the underlying physics of particulate foods consists in exploiting concepts from wet granular and composite materials flow (Heinrich et al., 2002; Mitarai and Noris, 2006; Behringer and Chakraborty, 2018). In this regard, a plethora of studies have been reported, and hence we examine only recent advances in the rheology of oil-continuous granular suspensions describable by theoretical approaches. Such systems are compositionally relevant to our model system. For a detailed account on the mechanics of particle-filled food gels or in general of granular suspensions with non-Newtonian matrices, the reader is referred to pertinent reviews (Guazzelli and Pouliquen, 2018; Scholten, 2017).

The rheology of chocolate, a semi-solid suspension of crumb powder dispersed in a fat continuous phase, has been shown to be reminiscent of dense hard-sphere suspensions (Blanco et al., 2019). The high-shear viscosity of the chocolate crumb powder η relative to the viscosity of oil-continuous phase η_0, obeys: $\eta_r = A\left(1-\frac{\phi}{\phi_m^{\sigma}(\sigma)}\right)^{-\lambda}$. Here, $A\simeq 1$ and $\lambda\simeq 2$ for spheres and the divergence of η_r towards infinity, occur at the maximum packing fraction ϕ_m, above which shear jamming occurs. The ϕ_m is a function of both the applied stress σ and the interparticle friction coefficient μ. For frictionless monodisperse spheres $\mu \to 0$, jamming occurs at random close packing $\phi_m = \phi_{rcp}$. For granular suspensions $\mu \gtrsim 1$, when an onset stress σ^* is exceeded, interparticle frictional contacts occur and η_r diverges at a maximum packing fraction $\phi_m < \phi_{rcp}$. In addition, interparticle adhesion introduces another stress scale σ_a. Modifying these parameters (e.g., by conching or adding surfactants) allows engineering ϕ_m, changing chocolate crumbs from a granular or powdery state to a fluid state.

The flow of biscuit creams and multicomponent milk molten chocolates has been described using a similar Maron-Pierce-Quemada (MPQ) model $\eta_r = \left(1-\frac{\phi}{\phi_m}\right)^{-2}$, but setting $\phi_m = \phi_{rcp}$ where ϕ_{rcp} is independently defined from a geometrical packing model, applied to non-attractive

* Corresponding author at: Unilever Innovation Centre Wageningen, Bronland 14, 6708 WH Wageningen, The Netherlands.
E-mail address: braulio.rodriguez@unilever.com (B.A. Macias-Rodriguez).

https://doi.org/10.1016/j.foostr.2022.100257
Received 6 May 2021; Received in revised form 30 November 2021; Accepted 17 January 2022
Available online 31 January 2022

hard- and soft-spheres (Farr and Groot, 2009; Shewan, Deshmukh, Chen, Rodrigues, Selway & Stokes, 2021). The maximum packing fraction deviates from its theoretical values $\phi_m < \phi_{rcp}$ when attractive interactions exist and the percolation threshold is reached, i.e. $\phi_m < \phi_{rcp}$, that leads to an filler volume-spanning network. The elasticity of such network is modelled according to percolation theory as: $G' = \beta(\phi\text{-}\phi_m)^{\alpha}$ where ϕ_m is obtained from the experimental viscosity data, considering size distribution effects, and α and β are parameters derived from free fitting.

In our study, we investigate the reinforcement effect of starch particles dispersed in a hydrophobic soft viscoelastic lipid (crystals dispersed in oil) continuous phase. Our system represents a progression from past studies focused on dense suspensions of monodisperse spheres, particles dispersed in nonpolar solvents and starch dispersed in polar solvents (Gravelle et al., 2021; Shewan et al., 2021; Richards, Guy, Blanco, Hermes, Poy & Poon, 2020; Blanco et al., 2019; Zhou et al., 1995; Frith and Lips, 1995).

We use a chemically modified starch as it is a ubiquitous filler in food suspensions, it is polydisperse: characteristic of a real granular material, and it is as a good model particle due to its rigidity, limited swelling and absence of gelatinization in non-aqueous solvent, so that phase volume corrections are avoided. Starch also lacks physical interactions with the lipid viscoelastic matrix nor interferes with its crystallization as demonstrated by rheology and X-ray diffraction experiments. We model the linear rheology: elastic modulus of our system according to phenomenological models for particulate-filled suspensions and relate it to the nonlinear rheology: yield stress and yield strain via a homogenization approach for hard-spheres suspended in soft solids. Remarkably, the mechanical response at linear and nonlinear modest and finite shear strains, can be predicted using simple scaling arguments based on particle volume fraction and maximum packing fraction. The maximum packing fraction was estimated based on a geometric theory of random close packing of polydisperse hard spheres. Our findings are relevant to sensory perception and processing of dense oil-continuous suspensions, where rigid filler addition is often sought to modulate stiffness and processability.

2. Materials and methods

2.1. Materials

Soybean oil and glyceryl tripalmitate (≥85%) were obtained from Sigma-Aldrich (Netherlands). Thermflo starch was obtained from Ingredion (UK). Thermflo® starch is a chemically modified maize starch with high tolerance to heat and shear. The mass and quoted densities of the materials: 0.92 g/cm^3 at 25 °C (soybean oil), 0.8901 g/cm^3 at 47 °C (supercooled tripalmitin) and 1.5 g/cm^3 (starch) were used to calculate volume fractions, discounting any air that may inadvertently introduced during sample preparation. For starch particles, their mass, having ~11% native moisture content, was taken into consideration when estimating volume fractions. Since starch particles do not dissolve nor swell in oil, their volume fraction is deemed constant in this solvent. Estimation of volume fractions introduces an error in the vicinity of ~5–10% even for highly monodisperse hard spheres (Poon et al., 2012).

2.2. Sample preparation

Lipid mixtures at fixed glyceryl tripalmitate volume fraction $\phi = 0.1$ were heated and hold at 70 °C for 5 min, well above tripalmitin melting peak temperature, ~54 °C. Starch was added at increasing $\phi = 0.1$–0.5 to the melt, and hold for an additional 5 min while stirring at 1000 min^{-1} with a Silverson head (1 mm screen for $\phi = 0.1$–0.4 and 1 cm screen for $\phi = 0.5$, Silverson) to ensure thermal equilibration and homogeneity of the samples. Suspensions (~100 g) were transferred to aluminum containers and rapidly cooled by bringing the samples to − 20 °C and held for 1 h to promote small crystal formation, and then brought to 20 ºC for crystal aggregation to ensue. Samples were manually stirred to maximize isotropic distribution of particles in the continuous medium and to eliminate air inadvertently introduced in the composites during mechanical mixing. However, no evidence of air bubbles was observed when samples were observed by microscopy. Measurements were performed after a week to allow any remnant crystallization and crystal Ostwald ripening to culminate.

2.3. Scanning electron microscopy (SEM)

High resolution SEM were conducted on a with Scanning Electron Microscopy (TM Hitachi 3000). The sample was sputtercoated with platinum (120 s) for a better SEM contrast and to prevent charging by the electron beam.

2.4. Transmitted light microscopy

Samples were carefully sandwiched between glass slides and cover slips and were visualized using via light microscopy (MOR2410, Malvern, United Kingdom) with a 5 × magnification objective. The microscopy was operated in bright-field and polarized modes. Samples were prepared on glass slides at similar melting and crystallization detailed in the Sample Preparation section. Sample volume (~1 g) may result in different heat/mass than samples prepared in “bulk”.

2.5. Confocal microscopy

Samples were visualized with a confocal laser scanning microscope (CLSM) (Zeiss, Oberkochen, German) with 20 × and 40 × magnification objectives. A fluorescent dye Nile Red was used to label the continuous oil phase. Oil was detected using a laser with 488 nm excitation wavelength respectively. Intensity data were collected at emission wavelength ranges of 600–680 nm. Images were collected at $\phi_{filler} = 0.1$–0.2 since higher vol. fraction preclude image acquisition due to multiple scattering. Micrographic ‘tiles’ of 25 pictures were collected and analyzed to determine the size distribution of the non-spherical starch granules according to their Feret’s statistical diameter, defined as the longest distance between two parallel planes restricting the object perpendicular to that direction. Micrographs tiles were processed in Fiji Image J (Version 1.52p) by applying an automatic threshold and watershed algorithm. Particle counting was determined using the analyze particle plugin, discarding particles in the edges (See Fig. S1 Supporting Information for higher magnification micrographs).

2.6. Particle size distribution

Size distributions of starch particles were carried out using laser diffraction with a Mastersizer 2000 equipped with ‘Scirocco’ and ‘Hydro’ units for dry powder dispersion and liquid dispersions (Malvern, UK). Particle were modelled as spheres and refractive indexes 1.54 and 1.47 were used for starch and soybean oil, respectively. The Mastersizer measurements were used to obtain the median particle size ($d_{0.5}$) of both dry powder and starch dispersed in oil, and the volume/mass moment mean (d_{43}) and the surface moment mean (d_{32}) of starch dispersed in oil. The values d_{43} and d_{32} providing information of the spread of the log-normal distribution $\sigma^2 = \ln(d_{43}/d_{32})$, are used to determine a maximum packing fraction ϕ_m assuming the most efficient packing of polydisperse hard spheres isotropically in 3D, that is the RCP density ϕ_{rcp}, based on a geometrical theory proposed by Farr ad Groot (2009). This theory validated by extensive numerical simulations, has been proven useful in predicting ϕ_m of colloidal and non-colloidal hard spheres with polydisperse size distributions (Farr ad Groot 2009; Shewan and Stokes, 2015). In using this theory, we treat starch particles as hard spheres, both with regards to their interaction potential and geometry, packing in a Newtonian-fluid: the molten lipid phase. Pertaining

these aspects, the theory corrects for a general but weak dependence of ϕ_{rcp} on fluid viscosity and particle size, by choosing a specific relation between mass and particle size, making ϕ_{rcp} well-defined. In addition, we argue that any geometrical anisotropy of the particles inflicted due to lipid crystallization could be 'erased' by mixing before loading, and that interparticle friction, causing $\phi_m < \phi_{rcp}$, would be only relevant at high stresses triggered by highly nonlinear deformations. For a detailed account of the theory, the reader is referred to Farr ad Groot (2009).

2.7. Powder X-ray diffraction

X-ray diffraction experiments were conducted to probe changes on nucleation/crystallization that would translate in changes on the mechanics of the lipid gel. Small-angle X-ray diffraction (SAXD) and Wide-angle X-ray diffraction (WAXD) were conducted on a laboratory scale Bruker D8 Discover X-ray powder diffractometer with a Väntec 500 2D detector and an IμS microfocus X-ray source (CuK α radiation, $\lambda = 0.154184$ nm). The diffraction patterns were collected in a transmission mode with the X-ray beam perpendicular to the flat sample surface. A 1-mm collimating slit was used and the sample to detector distance was 32.5 cm. A typical measurement time used was 900 s. SAXD and WAXD were collected in $2\theta = 1$–10° and $2\theta = 7$–55° ranges, respectively. One dimensional X-ray diffraction patterns were determined from the 2D images using the GADDS (version 1.28) software. The obtained X-ray diffraction patterns are imported in the Bruker EVA software (version 12.0) for peak identification and peak shape analysis. The average crystal thickness (ACT) was calculated by Scherrer equation based on the Full Width at Half Maximum (FWHM) values of the first order long-spacings of fats from the SAXD spectra (den Adel, van Malssen, van Duynhoven, Mykhaylyk & Voda, 2018). The polymorphism or spatial arrangement of the subcell structure was determined based on peak identification of short-spacings in the WAXD spectra (Himawan et al., 2006).

2.8. Shear rheology

Rheological properties were determined using a torque-controlled rheometer (MCR 302, Anton Paar GmbH, Germany) equipped with parallel-plate of DIA: 25 mm ($\phi_{filler} = 0.1$–0.4) and DIA: 10 mm ($\phi_{filler} = 0.5$) and with serrated geometries ($1 \times 1 \times 0.5$ mm serrated grid of truncated pyramids) to circumvent wall slip. In order to perform measurements of thixotropic materials such as lipid gels, with a reproducible initial state, samples were manually stirred during their preparation and rested for ~10 min post loading to allow relaxation of internal stresses. The manual mixing procedure was adopted to avoid shear-induced migration of particles, inadvertently introduced by preshear protocols, and to promote isotropic distribution of particles. Measurements were conducted at a fixed gap height of $h = 1$ mm, much larger than the mean granular size ~30 μm. For $\phi_{filler} = 0.5$, we fixed a constant normal force rather than a fixed gap as to avoid measuring artifacts. Exerting large normal forces during loading can increase the modulus up to an order of magnitude (See Fig. S4 Supporting Information). After slowly fixing the gap, the following procedure was applied: i) oscillations are applied within the linear regime $\gamma_0 = 0.01^{\%}$ and $\omega = 0.32$ 1/s for to obtain the steady-state plateau elastic modulus $G^{'}$; ii) a subsequent amplitude sweep $\gamma_0 = 10^{-3}$-$10^{3\%}$ at the same frequency or small rotational velocity ($\dot{\gamma} = 10^{-3}$ 1/s) are imposed to obtain the yield stress σ_y. The initial elasticity measurement is nonperturbative, except for $\phi_{filler} = 0.5$ where multiple linear pre-oscillations lead to an increase in $G^{'}$ (See Fig. S3 Supporting Information). Therefore, for $\phi_{filler} = 0.5$, we obtained only a steady state measuring point to obtain the linear modulus, and then carried out the same procedure as described above. To estimate the yield stress, we used three approaches for comparative purposes, and as it was not known a priori whether oscillatory shear would induce anisotropic structures to larger degree due to the application of multiple oscillatory cycles at each shear strain input than rotational shear. Irrespective of the measuring method, yield stress occurs when stress is maximal: $\sigma(R) = \frac{T}{2\pi HR^2}$ for a parallel plate of arbitrary R radius. Oscillatory strain curves were fitted with cubic splines, and yield stresses were empirically determined by interpolating at the 'critical' point where the linear elastic moduli $G^{'}(\phi) = 0.9\, G^{'}(\phi)$, that is where it drops 90% of its initial value, or at the 'flow point' where $G^{'} = G^{''}$. Rotational yield stress was determined by intersection of stress growth curves, considered as the total stress that triggers full flow of the pastes. The yield strain was empirically estimated at the 'critical' point where the linear elastic moduli $G^{'}(\phi) = 0.9\, G^{'}(\phi)$. Although arbitrary, this procedure was more sensitive to capture the effect of the filler on the onset of yielding. Approaches such as determining the yield strain from 'line intersections' of the elastic modulus, yield strain at the flow point $G^{'} = G^{''}$ or from stress-growth experiments were unsuccessful, as either the strain varied very little, or it was ill-defined. Some of the advantages and disadvantages of using these methods to determine the yield stress and strain have been recently reviewed (Dinkgreve, Paredes, Denn & Bonn, 2016). Elastic moduli and yield stresses of the pastes as a function of volume fraction of embedded particles were measured. Estimation of rheological measurements introduces an error in the range of ± 5–10%. Although serrated parallel plates were used for all measurements to minimize slip, high volume fractions $\phi_{filler} = 0.5$ show unsteady stick-slip flow or fracture above $\gamma_0 \approx 40\%$.

3. Results and discussions

Fig. 1 shows a representative sample of the filler particles: starch and the composite system: starch-filled gel. Starch particles appear as discrete granules or agglomerates with irregular shape and average grain size: $F \approx 10$ μm (median Feret's diameter from microscopy). Individual granules have high roundness of ~ 0.8. When treated as spheres, starch have an average size $d_{0.5} = 24.1 \pm 0.6$ μm (median spherical diameter from laser diffraction) in their powder state, whereas $d_{0.5} = 27.4 \pm 0.3$ μm in their solvent-dispersed state, confirming the absence of swelling in oil (Fig. 1b).

Fat crystal networks are known for their fractal nature and multiple length scales. Our CLSM microscopic images (Fig. S1) reveals the microstructure of the suspension comprised of a coarse fraction and a colloidal fraction. The coarse fraction is made up of optically dense, larger, rigid and non-interacting, (chemically modified) starch particles, whereas the colloidal fraction is made up (on average) of much smaller, less dense network of fat nanoscale plates forming soft and deformably clusters due to weak van der Waal interactions. We only observed isolated cases where large and dense fat crystal clusters were present (See Fig. S1 for higher magnification micrographs). Given these differences in length-scale and interaction potential, we can consider that the coarse fraction interacts with the colloidal fraction only through hydrodynamic interactions, i.e., starch particles see the lipid network as a homogeneous phase fluid. Moreover, we observe that starch dispersed in oil or lipid gels, and subjected to similar thermal/crystallization regimes share similar microstructure (Fig. 2a,b). Some degree of agglomeration is also observed likely a consequence of sandwiching the fat-starch dispersions between glass surfaces and excluded volume effects due to crystallization of the solid lipid phase upon cooling. Such particles agglomerates could be separated by ordinary shear and would not cause strong divergence from ϕ_{rcp}, as confirmed by rheology results. Birefringence is also present in starch and lipid, suggesting starch particles retain their integrity post thermal treatment due to their crosslinking nature and absence of water acting a plasticizer (Fig. 2c). This supports the notion that changes in phase volume of starch with and without thermal treatment are negligible.

Fig. 3 presents the linear viscoelastic moduli $G^{'}$, $G^{''}$ of the lipid colloidal gel at fixed volume fraction $\phi_{tripalmitin} = 0.10$ (Fig. 2a) as a function of frequency, and the time evolution of the elastic modulus of the pure paste $\phi_{starch} = 0$ compared to a sample embedded with starch

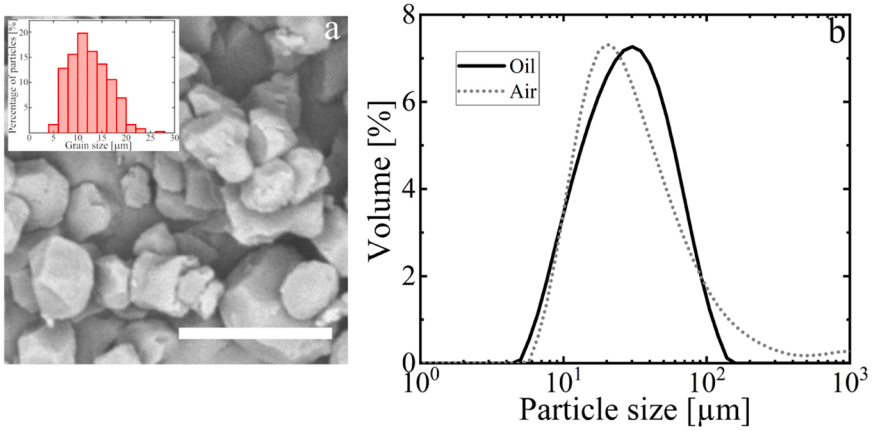

Fig. 1. (a) SEM micrograph of the Thermflo® starch and its corresponding grain size distribution (inset) as defined by Feret's diameter based on surface area of 2D confocal images (See Fig. S1 Supporting Information). (b) Particle size distribution of starch powder and starch in oil, treating particles as spheres. A tail in particle size distribution at $\gtrsim$ 100 μm is observed in the dry powder due to the presence of agglomerates, that disappear in oil dispersions.

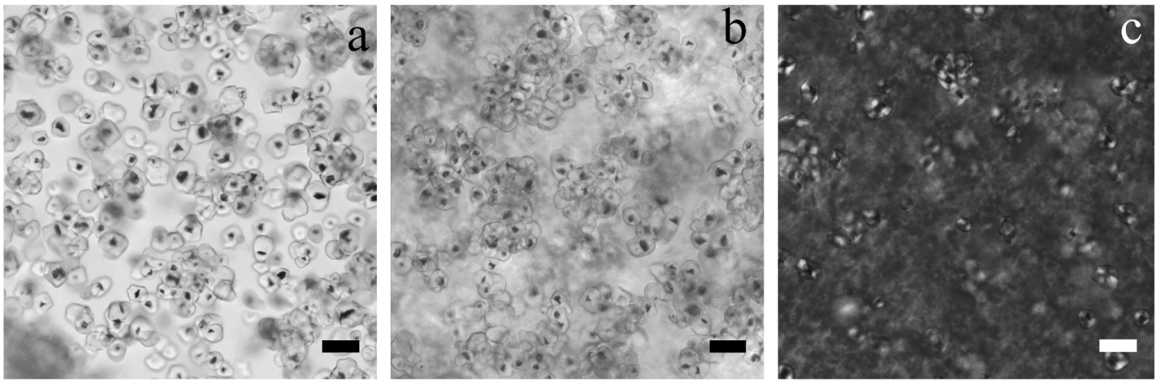

Fig. 2. Micrographs of starch in oil (a) and starch in lipid gel $\phi_{\text{tripalmitin}} = 0.10$ (b) at constant volume fraction $\phi_{\text{starch}} = 0.10$. Lipid crystal aggregates appear as floc-like aggregates. Polarized micrograph (c) of starch in lipid gel $\phi_{\text{tripalmitin}} = 0.10$. Scale bar in all figures equal 25 μm.

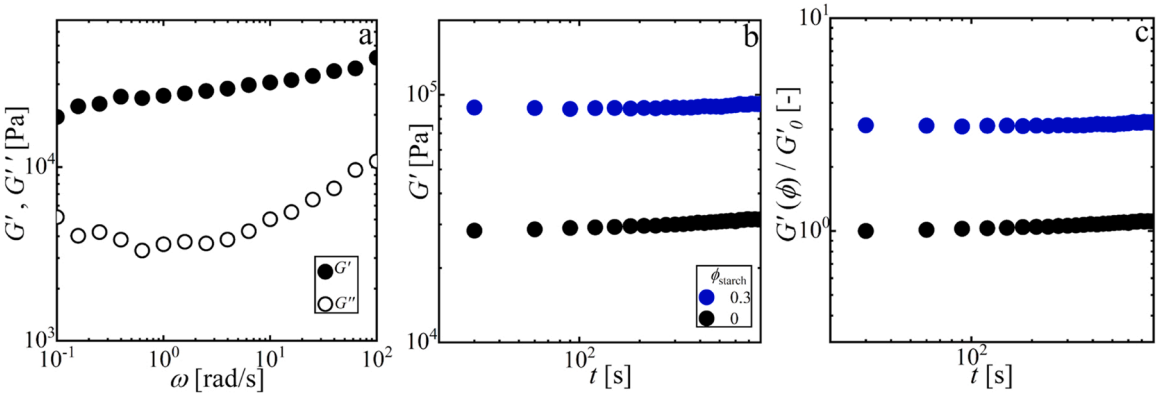

Fig. 3. Frequency sweep of the lipid viscoelastic gel at fixed volume fraction $\phi_{\text{tripalmitin}} = 0.10$ (a). Absolute elastic moduli (a) and dimensionless elastic moduli $G^{'}(\phi) / G^{'}_{0}$ (b) as a function of time, for representative samples with $\phi_{\text{starch}} = 0$ and $\phi_{\text{starch}} = 0.30$.

particles $\phi_{\text{starch}} = 0.3$. It is observed that $G^{'} > G^{''}$ displays weak frequency dependence as expected for soft solids. The elastic modulus $G^{'}$ weakly increases over time characteristic of thixotropic materials. We infer that any increase of $G^{'}$ with filler volume fraction ϕ as a function of time is due to structuration of the lipid phase, and in the absence of any physical interaction between the particle and paste, the time evolution of $G^{'}$ of the 'continuum' remains similar. This is supported by the absolute elastic moduli and dimensionless moduli normalized by $G^{'}_{0}$ at $\phi_{starch} = 0$ as function of time, which display similar structuring kinetics.

To further rule out starch-lipid molecular interactions, and the possibility of starch particles acting as catalytic nucleation sites, we demonstrate that neither average nanoplatelet crystal thickness: ACT (~ 40 nm) nor sub-cell packing: β polymorph, change substantially in the absence or presence of starch particles (See Fig. S2).

While the evolution of the mechanical properties with ϕ are nearly frequency-independent within the linear regime, the yield stress depends on the experimental timescale and the measuring method (Dinkgreve et al., 2016).

Next, we present the findings of the elastic modulus and yield stress/strain measurements as a function of starch granule volume fraction $\phi = 0–0.5$. We focus on these measures relevant to sensory perception: the elastic modulus and yield stress/strain are related to firmness and spreadability of oil-continuous suspensions, and industrial processes such as extrusion: e.g. yield stress (Macias-Rodriguez et al., 2018; Faber et al., 2017; Castro, Giles, Macosko & Moaddel, 2010). The impact of granular fillers embedded in the lipid gel on the mechanical properties, can be assessed by measurements of the linear elastic modulus $G^{'}$, yield stress σ_y and γ_y. Full strain amplitude oscillatory shear sweeps and stress-growth steady shear experiments at each volume fraction are included in Fig. 4. Oscillatory shear sweeps and steady shear stress-growth curves revealed a general trend: as particle volume fraction increases, composites gradually stiffen (increase in linear moduli and yield stress) and become brittle (decrease in yield strain) as ϕ approaches the maximum packing fraction ϕ_m. This visually appears as a transition from a soft paste to a firm paste to granulates. In what follows, we show that these essential mechanical features are akin to those of dense granular suspensions of hard-spheres.

First, we summarize (Fig. 5) these results performed on all samples with increasing volume fraction, focusing particularly on the evolution of dimensionless measures $G^{'}(\phi) / G^{'}(0)$ and $\sigma_y(\phi) / \sigma_y(0)$, to isolate the mechanical contribution of the particles to the paste. Both functions account for the mechanical strengthening of the material due to the presence of rigid inclusions. Absolute average values of the rheological measurements with their standard deviations are also presented. We note that all data points fall above a theoretical lower bound for the effective elastic moduli of quasi-isotropic and quasi-homogeneous biphasic materials given by Hashin and Shtrikman (1963):

$$\frac{G^{'}(\phi)}{G_0^{'}} > \frac{2+3\phi}{2-2\phi} \tag{1}$$

For infinitely rigid inclusions of arbitrary geometry, namely starch $G^{'} \approx 3$ GPa, dispersed in an elastic matrix such as a lipid gel $G^{'}_0 \approx 0.03$ GPa (Schroeter and Hobelsberger, 1992). The effect of the particle concentration on the elastic modulus is significant, even for low volume fraction of inclusions, we find $G'(\phi) \approx 1.5 \times G'_0$ for $\phi = 20\%$ and $G'(\phi) \approx 24.4 \times G'_0$ for $\phi = 50\%$ as the systems approaches its maximum packing fraction. Most phenomenological models addressing granular suspension problems involve homogenization techniques, which identify macroscopic properties from a material (comprising continuous and dispersed phases) treated as a continuum medium undergoing affine shear. These models differ from recent approaches considering heterogeneous stress deformation across the multiscale continuous phase (Gravelle and Marangoni, 2021).

Examples of the former type of models include Krieger-Dougherty (Eq. 2), Mendoza (Eq. 3) and Maron-Pierce type models (Eq. 4).

$$\frac{G^{'}(\phi)}{G_0^{'}} = \frac{1}{(1-\phi/\ \phi_m)^{2.5\phi_m}} \tag{2}$$

$$\frac{G^{'}(\phi)}{G_0^{'}} = \frac{1}{(1-\phi_{excl})^{2.5}},\ \phi_{excl} = \frac{\phi}{1-[(1-\phi_m)\phi/\phi_m]} \tag{3}$$

$$\frac{G^{'}(\phi)}{G_0^{'}} = \frac{1}{(1-\phi/\phi_m)^2} \tag{4}$$

Note that these models preserve their original form used to describe the relative viscosity of hard-sphere suspensions, except that the term denoting the relative viscosity η / η_0 is substituted by a term denoting the relative shear modulus $G^{'}(\phi) / G^{'}_0$. Such modifications have been used to describe the rheology of hard-spheres embedded in viscoelastic, glassy, gel and polymer matrixes (Guazzelli and Pouliquen, 2018; Pal, 2002). The first two models (Eqs. 3 and 4) reduce to Einstein's equation in the dilute regime $G^{'}(\phi) / G'_0 = 1 + 2.5\phi$, a reason of why they are favored by many researchers. However, the error of the Maron-Pierce and Einstein in the low volume fraction regime is not significant and is within the experimental error. Remarkably, we observe that all models provide good empirical predictions for the relative modulus of starch suspensions as a function of volume fraction if freely fitted by adjusting ϕ_m (See Fig. S4 Supporting Information). However, a major problem with free-fitting is that ϕ_m is inherent to the formulae: $\phi_m = 0.65$, $\phi_m = 0.72$ and $\phi_m = 0.73$ for Krieger-Dougherty, Maron-Pierce and Mendoza models, respectively. Equally important, empirically fitting ϕ_m is highly sensitive to experimental errors particularly close to the jamming transition where measuring the linear modulus or yield stress becomes increasingly difficult, due to particle-particle contacts and surface fracture. To illustrate, we applied increasing normal forces during sample loading which contributes to the stress response and increases $G^{'}$ by up to one-fold (See Fig. S3 Supporting Information). This artifact, likely caused by non-isotropic distribution and contacts as particles are pushed towards the parallel plate edges, augments with larger geometries due to increased surface area (See Fig. S3 Supporting Information). Past work suggests that particles contacts become predominant at $\phi \gtrsim 0.40$ and $\phi \gtrsim 0.48$ for frictional and frictionless monodisperse hard spheres, respectively (Guazzelli and Pouliquen, 2018). Fitting empirically the data with various $G^{'}$ at $\phi = 0.50$ leads to $\phi_m = 0.51–0.65$, where $\phi_m = 0.53$ is comparable to $\phi_m = 0.57$ reported for suspensions of granular monodisperse spherical particles in Non-Newtonian fluids (See Supporting Information; Mahaut, Chateau, Coussot & Ovarlez, 2008). This is somewhat surprising, as theory

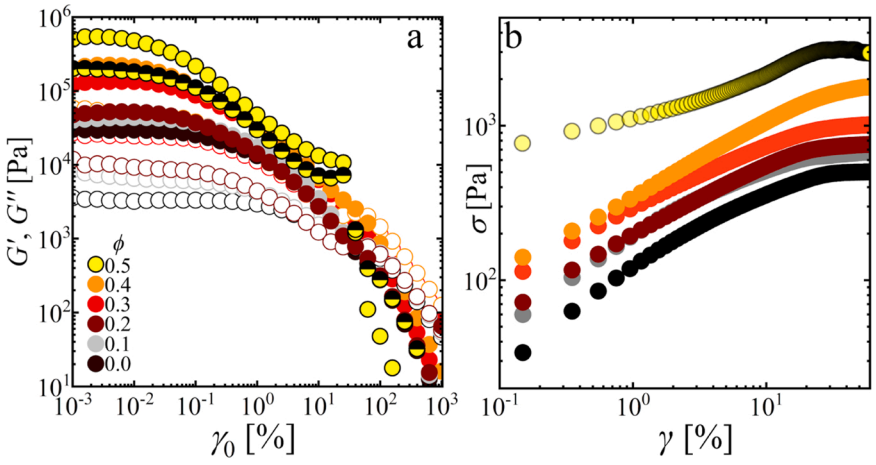

Fig. 4. Oscillatory shear rheology curves (a) and stress growth curves (b) at increasing volume fraction of starch $\phi = 0–0.50$. Constant frequency $\omega = 0.32$ 1/s and constant steady shear rate $\dot{\gamma} = 10^{-3}$ 1/s were applied during oscillations and rotations, respectively.

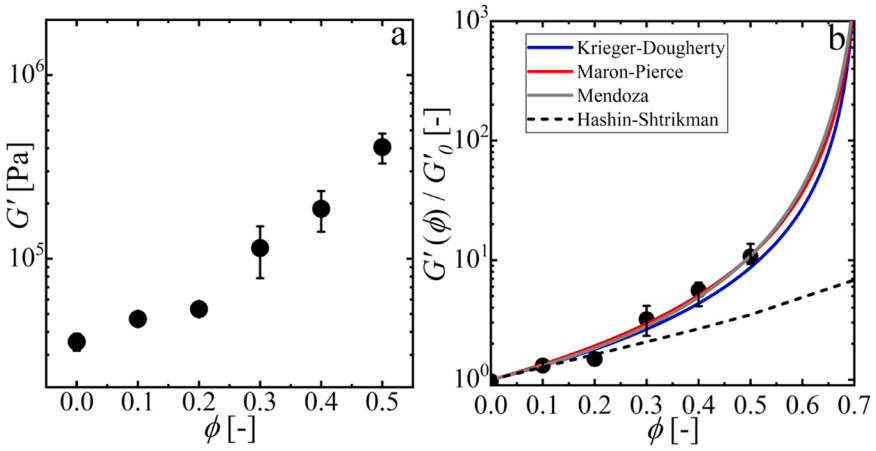

Fig. 5. Absolute linear elastic modulus G' (a), and dimensionless elastic modulus $G^{'}(\phi) / G^{'}_{0}$ (b) as function of starch volume fraction ϕ. Volume fraction of the solid lipid phase remained fixed at $\phi = 0.10$. All models are forced-fitted with a theoretical maximum packing fraction $\phi_m = 0.72 \pm 0.01$.

predicts that mixtures of particles with difference size can pack more densely than monodispersed particles (Desmond and Weeks, 2014; Far and Groot 2006). We therefore opted to use an alternative approach: calculate a theoretical ϕ_m independently from the log-normal distribution according to Farr and Groot (2006) and set the average ϕ_m with its standard deviation as upper/lower bounds for fitting all models. From the geometrical theory of polydisperse hard spheres, we estimated a much larger $\phi_m = 0.72 \pm 0.01$ assuming random close packing, using $d_{43} = 35.5 \pm 2.0$ and $d_{32} = 21.0 \pm 0.2$ of starch dispersed in liquid oil from laser diffraction experiments (Fig. 1). The ϕ_m estimated here is lower to the theoretical ϕ_m of polydisperse cubelike sugar granules (for monodisperse cubes $\phi_{rcp} = 0.78$) but much higher to the experimentally determined (via rheology) ϕ_m of cornstarch particle in oil ($\phi_m \lesssim 0.60$) (Shewan et al., 2021; Blanco et al., 2019). We find that forced setting of the model parameters leads to excellent predictions of the experimental data, with the Maron-Pierce and Mendoza models providing more accurate predictions $R^2 = 0.99$ than the Krieger-Dougherty model $R^2 = 0.91$. The good agreement of the models with our experimental data supports the notion that the elasticity of a suspension of rigid particles in a non-Newtonian soft solid is analogous to the problem of the viscosity a suspension of rigid particles in a Newtonian fluid, as shown in past studies (Guazzelli and Pouliquen, 2018).

Now, we turn our attention to the yield stress of the suspensions obtained using oscillatory shear and rotational shear measurements. In Fig. 6, we plot values of absolute yield stress σ_y (ϕ) and dimensionless yield stress σ_y (ϕ) / σ_0, and observed a similar qualitative trend irrespective of measuring method: the yield stress is less sensitive to the inclusion of granular fillers than the linear elastic moduli, e.g. we find σ_y (ϕ) $\approx 1.3 \times \sigma_0$ for $\phi = 20\%$ and σ_y (ϕ) $\approx 3 \times \sigma_0$ for $\phi = 50\%$. However, we find in all cases that the oscillatory yield stress at $G^{'} = G^{''}$ and that the rotational yield stress are over one order of magnitude larger than the oscillatory yield stress at 0.9 $G^{'}$. We do find differences in the absolute values of σ_y as these values are measurement dependent (Dinkgreve et al., 2016).

Establishing a relationship between the dimensionless elastic modulus and the dimensionless yield stress is challenging as the result depends on the micromechanical scheme utilized. An approach relevant to our model system is the homogenization approach discussed in Chateau et al., (2008):

$$\frac{\sigma_y(\phi)}{\sigma_0} = \sqrt{(1-\phi)\frac{G^{'}(\phi)}{G^{'}_{0}}} \tag{5}$$

In this type of mean-field like approach, the addition of particles induces amplification of stresses due to steric effects which increase the local shear rate of the interstitial paste or fluid, more than the macroscopic shear rate of the whole composite. The micromechanical estimate of this model is based on various assumptions including: (i) filler particles are rigid, monodisperse and noncolloidal spheres, (ii) amplification of shear rate occurs in the interstitial fluid and not at particle contacts, (iii) the distribution of the particles is isotropic and (iv) physical interactions between the particles and the continuous phase are

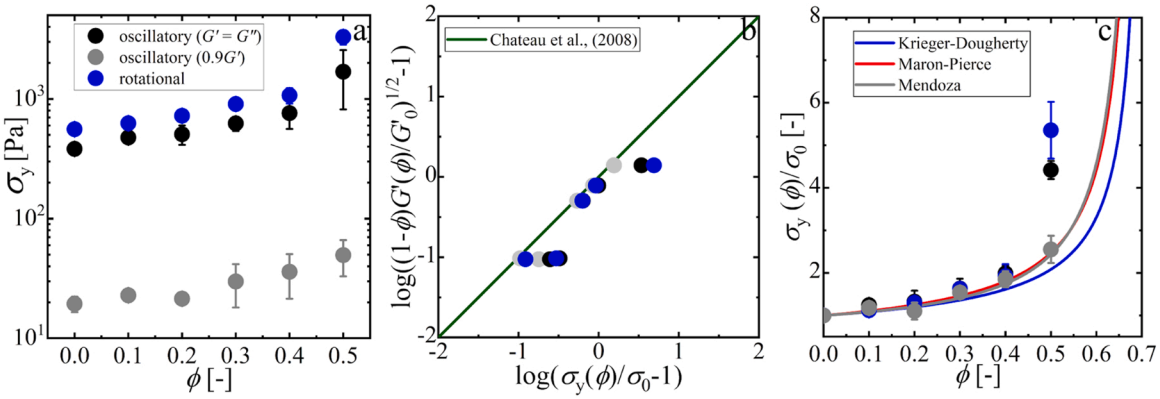

Fig. 6. Absolute yield stress σ_y vs. filler volume fraction, as measured by oscillatory and rotational shear (a). Dimensionless yield stress σ_y (ϕ) / σ_0 vs. dimensionless elastic modulus (b), described in Eq. (5) and symbolized by the green straight line. Dimensionless yield stress σ_y vs. filler volume fraction (c), fitted to Eq. (6) and modifications thereof for each phenomenological model, with maximum packing fraction $\phi_m = 0.72 \pm 0.01$. For $\phi = 0.50$, only σ_y at the onset of yielding (0.9 G') is considered for fitting, as other measures trigger particle-particle contacts.

absent, which we have demonstrated to be the case. Even if our particle fillers do not strictly comply with all these geometrical postulates, e.g., starch particles are polydisperse spheroids and not monodisperse spheres, it is possible to test experimentally the validity of the theoretical predictions against our model systems.

In Fig. 6b, we plot the dimensionless yield stress $\sigma_y(\phi) / \sigma_0$ as a function of the dimensionless elastic modulus $\sqrt{(1\text{-}\phi)G'(\phi)/G'_0}$ for all the systems studied in logarithmic coordinates. We observe that that there is a good agreement between our results and the micromechanical estimation of Eq. 5. Combining Eq. 2 and Eq. 3, the yield stress equation reads:

$$\frac{\sigma_y(\phi)}{\sigma_0} = \sqrt{\frac{1\text{-}\phi}{(1\text{-}\phi/\phi_m)^{2.5\phi_m}}} \quad (6)$$

Note that Eq. 6 is in the form of the Krieger-Dougherty model. For the Maron-Pierce model, "2" replaces the exponent "2.5 ϕ_m". For the Mendoza model the excluded volume fraction ϕ_{excl} substitutes the reduced volume fraction ϕ/ϕ_m and ϕ_m is dropped from the exponent "2.5 ϕ_m". Using $\phi_m = 0.72 \pm 0.01$, we found that all models capture reasonably well the experimental data, with the Maron-Pierce ($R^2 = 0.92$) and Mendoza ($R^2 = 0.90$) models providing more accurate predictions than Krieger-Dougherty ($R^2 = 0.74$). However, we observe that the oscillatory yield stress determined at the flow point $G' = G''$ and the rotational yield stress at $\phi \approx 0.50$, dramatically deviates from theoretical predictions. These features suggest that at $\phi \lesssim 0.40$, we always probe yielding to a frictionless state, whereas for $\phi \gtrsim 0.40$ this is only true for modest nonlinear deformations $\sigma_y = 0.9\ G^{'}$. In this regard, it has been suggested that steady shear, e.g., from rotational tests in our study, at moderate-to-dense volume fractions $\phi \approx 0.35$–0.60 probes frictional contacts, whereas oscillatory shear removes or relaxes contacts between non-Brownian corn-starch particles dispersed in oil (Richards et al., 2020). In our study, such contacts are activated at a critical nonlinear stresses σ^* and high-volume fractions $\phi \gtrsim 0.40$, as contacts might not be easily mobilized due to the presence of a dense lipid phase.

In Fig. 7, we plot values of the critical yield strain $\gamma_y(\phi)$ and the dimensionless yield strain $\gamma_y(\phi) / \gamma_0$ at the onset of yielding. We selected this measure as other approaches to determine the yield strain were unsuccessful as noted in the Materials and Methods section "Rheology". We observed that as starch volume fraction increases, the particle-filled gels become gradually more brittle, e.g. we find that $\gamma_y(\phi) / \gamma_0$ drops almost an order of magnitude as ϕ_{starch} increases from 0% to 50%. As $\gamma_y(\phi) \approx \sigma_y(\phi) / G^{'}(\phi)$, the adimensional yield strain obeys a similar scaling law:

$$\frac{\gamma_y(\phi)}{\gamma_0} = \sqrt{(1\text{-}\phi)(1\text{-}\phi/\phi_m)^{2.5\phi}} \quad (7)$$

Here, Eq. 7 is in the form of the Krieger-Dougherty model. For the Maron-Pierce model, "2" replaces the exponent "2.5 ϕ_m". For the Mendoza model the excluded volume fraction ϕ_{excl} substitutes the reduced volume fraction ϕ/ϕ_m and ϕ_m is dropped from the exponent "2.5 ϕ_m". Using $\phi_m = 0.72 \pm 0.01$, we see that the scaling law describes remarkably well the experimental trends, with a least square fitting $R^2 = 0.99$ for all models.

Overall, the experimental data agrees well with the theoretical predictions from homogenization analysis for monodisperse hard spheres suspended in yield-stress fluids, even when our particles depart from 'ideality'. Although we did not systematically investigate the effect of starch from other sources or edible fillers with varying size distribution, we speculate that similar scaling will hold for spheroid rigid fillers up to $\phi \approx 0.40$–0.50 if ϕ_m is estimated for different particle populations (Molenda, Stasiak, Horabik, Fornal, Blaszczak & Ornowski, 2006). For $\phi \gtrsim 0.50$, a phenomenological model which takes into consideration the contribution of finite-size contacts, e.g. friction, to the stress response appears more suitable. The extent and onset of friction will be dependent on the type of flow, oscillatory versus steady shear, and plausibly on the yield stress of the continuous lipid phase (Richards et al., 2020). Pertaining the latter, at low ϕ lipid crystals could act as lubricants relaxing interparticle contacts, whereas at high ϕ could serve as "blockers" immobilizing interparticle contacts. These aspects merit further investigation. Finally, it is noteworthy that the impact of granular fillers on gels contrasts from colloidal fillers, where both the elastic moduli and yield stress are expected to obey roughly the same scaling with volume fraction.

4. Conclusions

We have investigated experimentally the mechanical contribution of rigid polydisperse starch particles to lipid crystal networks. We focused on the influence of volume fraction on the elastic modulus, yield stress and yield strain of the suspensions. As the filler volume fraction increases, the starch-filled lipid gels gradually stiffen, become brittle and granulate, as $\phi \to \phi_m$. The dimensionless elastic modulus $G'(\phi) / G^{'}_0$ depends on starch volume fraction ϕ and obey similar phenomenological models used to describe the viscosity of hard-sphere suspensions, such as the Maron-Pierce model: $(1 - \phi/\phi_m)^{-2}$ with a maximum volume fraction $\phi_m = \phi_{rcp}$ of polydisperse hard-spheres. The maximum volume fraction dependent on the "kind" of particle, $\phi_m = 0.72 \pm 0.01$, is determined independently from a geometry theory of RCP for polydisperse hard spheres, based on the log normal distribution of starch

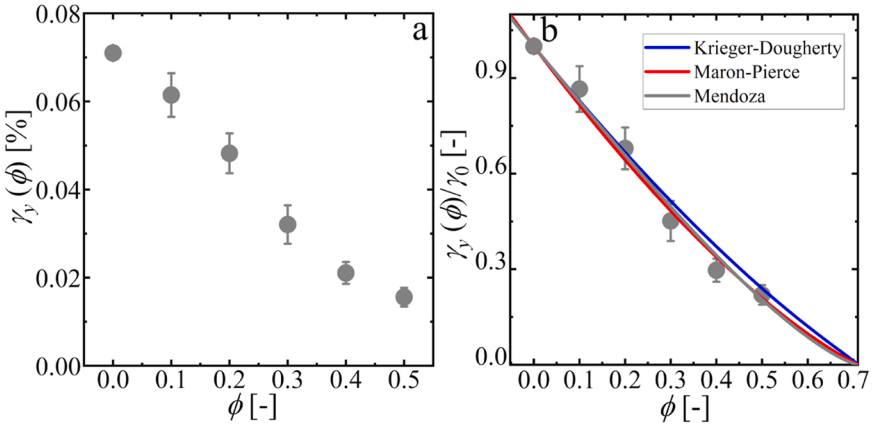

Fig. 7. Absolute yield strain γ_y (a) and dimensionless yield strain $\gamma_y(\phi) / \sigma_0$ vs. filler volume fraction, as measured by oscillatory and rotational shear. Dimensionless yield strain (b) fitted to Eq. (6) and modifications thereof for each phenomenological model with maximum packing fraction $\phi_m = 0.72 \pm 0.01$.

particles dispersed in oil. The yield stress/concentration are related to the elastic modulus/concentration relationship through a simple scaling law: $\sigma(\phi)/\sigma_0 = \sqrt{(1\text{-}\phi)G'(\phi)/G'_0}$ derived from a homogenization approach based on hydrodynamic interactions of monodisperse hard spheres within a soft viscoelastic medium. From this scaling law, the yield strain/concentration relation to the elastic modulus/concentration is also determined as $\gamma_y(\phi) \approx \sigma_y(\phi) / G'(\phi)$. We hypothesize that similar relationships will hold for other granular passive fillers integrated in concentrated food suspensions up to $\phi \approx 0.40$–0.50, after which contact forces may predominate. These scaling laws could also help to predict the effect of fillers on sensory attributes and processing of such pastes.

Associated content

Additional confocal micrographs, X-ray diffraction patterns and rheological measurements are included in the Supporting Information, which is available free of charge.

Declaration of Competing Interest

The authors declare that they have no known competing financial interests or personal relationships that could have appeared to influence the work reported in this paper.

Acknowledgments

The authors thank Ziya Lan and Ruud den Adel for conducting part of the rheological experiments, and X-ray diffraction measurements, respectively, presented in this work. Robert Farr is also acknowledged for providing us with the "SpherePack1D" code used to calculate ϕ_{rcp}, and for useful discussions. We also thank Professor Daniel Bonn for his insights while preparing this article. This project has received funding from the European Union's Horizon 2020 research and innovation programme under the Marie Sklodowska-Curie grant agreement No. 798917.

Appendix A. Supporting information

Supplementary data associated with this article can be found in the online version at doi:10.1016/j.foostr.2022.100257.

References

den Adel, R., van Malssen, K., van Duynhoven, J., Mykhaylyk, O. O., & Voda, A. (2018). Fat crystallite thickness distribution based on SAXD peak shape analysis. *European Journal of Lipid Science and Technology, 120*(9), Article 1800222.

Behringer, R. P., & Chakraborty, B. (2018). The physics of jamming for granular materials: a review. *Reports on Progress in Physics, 82*(1), Article 012601.

Blanco, E., Hodgson, D. J., Hermes, M., Besseling, R., Hunter, G. L., Chaikin, P. M., & Poon, W. C. (2019). Conching chocolate is a prototypical transition from frictionally jammed solid to flowable suspension with maximal solid content. *Proceedings of the National Academy of Sciences, 116*(21), 10303–10308.

Castro, M., Giles, D. W., Macosko, C. W., & Moaddel, T. (2010). Comparison of methods to measure yield stress of soft solids. *Journal of Rheology, 54*(1), 81–94.

Chateau, X., Ovarlez, G., & Trung, K. L. (2008). Homogenization approach to the behavior of suspensions of noncolloidal particles in yield stress fluids. *Journal of Rheology, 52*(2), 489–506.

Desmond, K. W., & Weeks, E. R. (2014). Influence of particle size distribution on random close packing of spheres. *Physical Review E, 90*(2), Article 022204.

Dinkgreve, M., Paredes, J., Denn, M. M., & Bonn, D. (2016). On different ways of measuring "the" yield stress. *Journal of non-Newtonian fluid mechanics, 238*, 233–241.

Faber, T. J., Van Breemen, L. C. A., & McKinley, G. H. (2017). From firm to fluid–structure-texture relations of filled gels probed under large amplitude oscillatory shear. *Journal of Food Engineering, 210*, 1–18.

Farr, R. S., & Groot, R. D. (2009). Close packing density of polydisperse hard spheres. *The Journal of chemical physics, 131*(24), Article 244104.

Frith, W. J., & Lips, A. (1995). The rheology of concentrated suspensions of deformable particles. *Advances in colloid and interface science, 61*, 161–189.

Genovese, D. B. (2012). Shear rheology of hard-sphere, dispersed, and aggregated suspensions, and filler-matrix composites. *Advances in colloid and interface science, 171*, 1–16.

Gravelle, A. J., & Marangoni, A. G. (2021). A new fractal structural-mechanical theory of particle-filled colloidal networks with heterogeneous stress translation. *Journal of Colloid and Interface Science, 598*, 56–68.

Guazzelli, É., & Pouliquen, O. (2018). Rheology of dense granular suspensions. *Journal of Fluid Mechanics, 852*, P1.

Hashin, Z., & Shtrikman, S. (1963). A variational approach to the theory of the elastic behaviour of multiphase materials. *Journal of the Mechanics and Physics of Solids, 11*(2), 127–140.

Heinrich, G., Klüppel, M., & Vilgis, T. A. (2002). Reinforcement of elastomers. *Current opinion in solid state and materials science, 6*(3), 195–203.

Himawan, C., Starov, V. M., & Stapley, A. G. F. (2006). Thermodynamic and kinetic aspects of fat crystallization. *Advances in colloid and interface science, 122*(1–3), 3–33.

Macias-Rodriguez, B. A., Ewoldt, R. H., & Marangoni, A. G. (2018). Nonlinear viscoelasticity of fat crystal networks. *Rheologica Acta, 57*(3), 251–266.

Mahaut, F., Chateau, X., Coussot, P., & Ovarlez, G. (2008). Yield stress and elastic modulus of suspensions of noncolloidal particles in yield stress fluids. *Journal of Rheology, 52*(1), 287–313.

Mitarai, N., & Nori, F. (2006). Wet granular materials. *Advances in Physics, 55*(1–2), 1–45.

Molenda, M., Stasiak, M., Horabik, J., Fornal, J., Blaszczak, W., & Ornowski, A. (2006). Microstructure and mechanical parameters of five types of starch. *Polish Journal of Food and Nutrition Sciences, 15*(2), 161.

Pal, R. (2002). Complex shear modulus of concentrated suspensions of solid spherical particles. *Journal of colloid and interface science, 245*(1), 171–177.

Poon, W. C., Weeks, E. R., & Royall, C. P. (2012). On measuring colloidal volume fractions. *Soft Matter, 8*(1), 21–30.

Richards, J. A., Guy, B. M., Blanco, E., Hermes, M., Poy, G., & Poon, W. C. (2020). The role of friction in the yielding of adhesive non-Brownian suspensions. *Journal of Rheology, 64*(2), 405–412.

Scholten, E. (2017). Composite foods: from structure to sensory perception. *Food & function, 8*(2), 481–497.

Schroeter, J., & Hobelsberger, M. (1992). On the mechanical properties of native starch granules. *Starch-Stärke, 44*(7), 247–252.

Shewan, H. M., Deshmukh, O. S., Chen, G., Rodrigues, S., Selway, N., & Stokes, J. R. (2021). Interpreting rheological behaviour of sugar-fat mixtures as a function of solids phase volume. *Journal of Food Engineering, 297*, Article 110474.

Shewan, H. M., & Stokes, J. R. (2015). Analytically predicting the viscosity of hard sphere suspensions from the particle size distribution. *Journal of Non-Newtonian Fluid Mechanics, 222*, 72–81.

Wijmans, C., & Dickinson, E. (1998). Brownian dynamics simulations of filled particle gels. *Journal of the Chemical Society, Faraday Transactions, 94*(1), 129–137.

Zhou, J. Z., Uhlherr, P. H., & Luo, F. T. (1995). Yield stress and maximum packing fraction of concentrated suspensions. *Rheologica acta, 34*(6), 544–561.